Tunneling Voltage Polarity Dependent Submolecular Contrast of Naphthalocyanine on Graphite. A STM Study of Close-Packed Monolayers under Ultrahigh-Vacuum Conditions

Markus Lackinger,[†,‡] Thomas Müller,[†] T. G. Gopakumar,[‡] Falk Müller,[‡] Michael Hietschold,[‡] and George W. Flynn*[,†]

Department of Chemistry and Columbia Center for Integrated Science and Engineering, Columbia University, New York, New York 10027, and Institute of Physics, Chemnitz University of Technology, D-09107 Chemnitz, Germany

Received: September 9, 2003; In Final Form: November 25, 2003

Self-assembled monolayers of free-base naphthalocyanine are examined in the context of analogous phthalocyanine films, revealing the influence of the more extended π-electron system on monolayer properties. Naphthalocyanine was vapor-deposited on a graphite substrate in ultrahigh vacuum and investigated in situ at low temperature (50 K) using scanning tunneling microscopy (STM). The crystallographic monolayer parameters of the deposited films were determined by means of submolecularly resolved STM images. In addition, vacancies in the monolayer have allowed for an accurate measurement of single molecule azimuthal angles. In STM topographs with submolecular resolution, a clear difference is evident between tunneling images corresponding to occupied and unoccupied sample states. The intramolecular structure exhibited by the STM images can be understood qualitatively by considering frontier orbitals calculated for isolated molecules. Moreover, single point tunneling spectra show a distinct signature of the organic adlayer as expected for resonant tunneling.

Introduction

The structure of naphthalocyanine (Nc) is depicted in the inset of Figure 1. Nc can be considered to be an enlarged derivative of phthalocyanine (Pc) with additional benzo groups at each of the four benzopyrrole groups, providing a more extended π-electron system. Free-base Nc is a planar molecule lacking any external functional groups to enhance specific intermolecular interactions, which consist largely of relatively weak van der Waals forces. The core of the molecule is identical to that of phthalocyanine and can be modified with substituents such as divalent metal atoms or different complexes at the central binding site. Like phthalocyanines, Nc exhibits both high thermal and chemical stability and low vapor pressure at room temperature, making the molecule suitable for deposition by vacuum sublimation.

Phthalocyanines and their possible device applications have been at the center of numerous studies due to their interesting electrical and optical properties. The electronic structure of these molecules (e.g., HOMO−LUMO gap, redox potential) can be tuned through metal substitution at the central binding site and ring derivatization, thus affording great versatility in controlling molecular properties. Due to its sensitivity to electronic structure, scanning tunneling microscopy (STM) is a powerful tool for investigating thin films of these species. Copper phthalocyanine (CuPc) was among the first molecules ever imaged[1,2] and has been intensively investigated by STM on a variety of crystalline substrates with different coverages.[3−14] In the case of planar metal substituted Pc, the apparent height of the molecular center in the STM profile is crucially dependent on the chemical nature of the central metal atom. Hence, both CuPc/CoPc [15,16] and NiPc/FePc [17] can be distinguished by their internal structure when adsorbed on a Au(111) substrate, due to differences in the electronic structure of the central metal atom substituent. Thus, chemical sensitivity is attained with the STM for selected mixed molecular layers of these molecules. Furthermore, nonplanar metal substituted phthalocyanines PbPc [18] and SnPc [19] exhibit two different adsorption geometries that can be distinguished by STM imaging with submolecular resolution. So far, there have been few reported imaging studies of Nc in the literature. For layers of FeNc several nanometers thick on an amorphous carbon substrate,[20] ZnNc on MoS_2 [21] and CoNc on NaCl,[22] the molecules are reported to adsorb with their plane perpendicular to the surface and the stacking axis parallel to the substrate. On the other hand for vanadyl-Nc on HOPG, a stacking axis perpendicular to the substrate and slightly tilted molecules have been proposed.[23] None of these studies has dealt with the morphology of the first monolayer, and submolecular resolution was not attained.

Due to the absence of any additional functional groups, intermolecular and molecule−substrate interactions are essentially the same for Nc monolayers as for their Pc counterparts, thereby making Nc a suitable model system in which to study the influence of molecular size on the self-assembly process. Moreover, the presence of a fairly extensive conjugated electron system suggests that Nc is a promising candidate for molecular electronics applications. Compared to Pc, the more extended, conjugated electron system of Nc influences the energies of the molecular orbitals and is expected to lead to a smaller HOMO−LUMO gap. As with Pc, metal substitution at the central binding site may facilitate further manipulation of the electronic structure. In analogy to Pc monolayers, distinct (i.e., chemically specific) STM signatures[15−17] may be expected for the substituted Nc species, and the present study has indeed uncovered a remarkably rich tunneling behavior for free-base Nc.

* To whom correspondence should be addressed. Telephone: 212-854-5026. Fax: 212-854-8336. E-mail: flynn@chem.columbia.edu.
[†] Columbia University.
[‡] Chemnitz University of Technology.

10.1021/jp036698v CCC: $27.50
Published on Web 01/16/2004

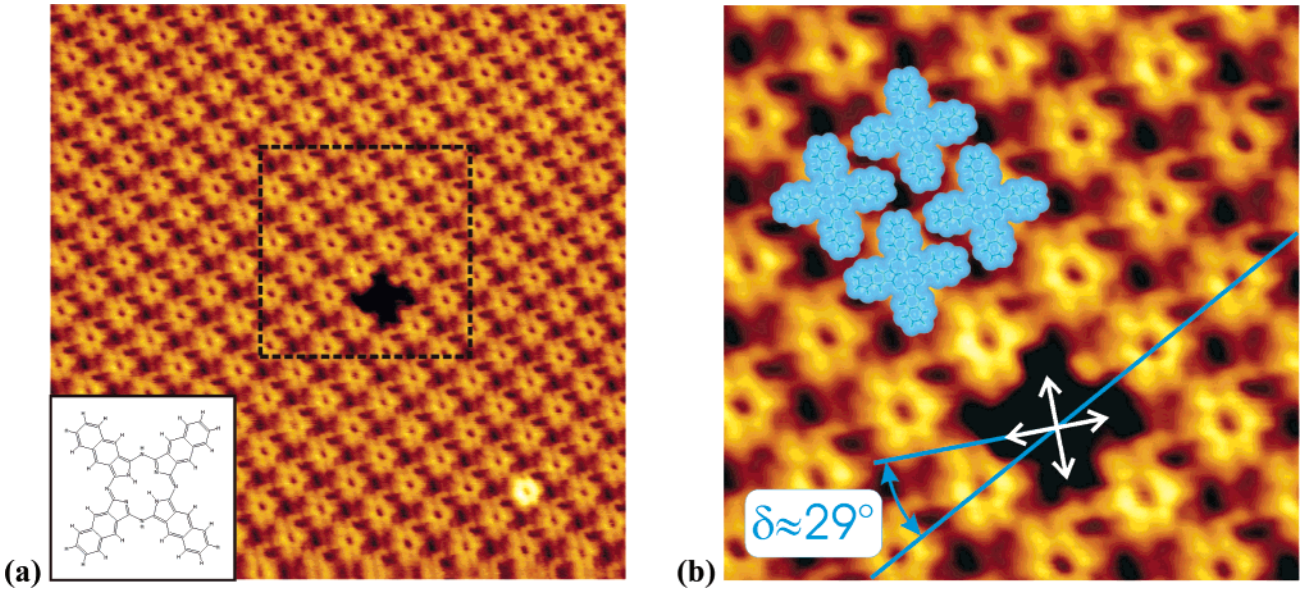

Figure 1. (a) STM constant current topograph of Nc on HOPG (25×25 nm^2, -1.83 V, 83 pA) obtained at a surface temperature of approximately 50 K. The otherwise close packed monolayer exhibits a single vacancy, which allows the azimuthal orientation of single molecules within the layer to be determined; the inset in a shows the structure of naphthalocyanine ($C_{48}H_{26}N_8$). (b) Expanded section (mean filtered, 9×9 nm^2) as marked in a. An angle of 29° between the molecular axis and the lattice vector was measured; this orientation was applied to overlay the model unit cell shown in the upper left part of the figure.

Experimental Section

All experiments were conducted under ultra-high-vacuum conditions with a base pressure of $\sim 2 \times 10^{-10}$ mbar. The vacuum system was equipped with an ion gun, rear view low-energy electron diffraction (LEED) optics (Princeton Research Instruments), and a commercial VT STM (Omicron GmbH). The films were prepared in situ by vacuum sublimation in a small extension chamber attached to the main bell jar. For the deposition a thermally shielded home-built evaporator with a molybdenum crucible and a type K (chromel−alumel) thermocouple was used. Nc was supplied by Aldrich with a purity of 97% and used without further ex-situ purification. Prior to deposition, the evaporant was outgassed at a temperature slightly above the 480 °C used for evaporation. The deposition rate was monitored with a quartz microbalance, which was calibrated by subsequent LEED and STM measurements. Very low evaporation rates were employed, resulting in a deposition time of about 5 min for the first monolayer. Highly oriented pyrolytic graphite was freshly cleaved and immediately introduced into the vacuum system. To desorb the remaining contaminants, the substrate was cleaned several times by in situ heating to approximately 700 °C for 20 min. For STM measurements the sample was cooled with a liquid helium flow cryostat to sample temperatures of ~50 K with the tip remaining near room temperature. STM tips were prepared by electrochemical ac etching of a polycrystalline tungsten wire. Ultrahigh-vacuum Ar^+-ion sputtering and annealing to 700 °C provided clean, stable tips capable of submolecular resolution. All images shown were taken in the constant current mode of operation and some are mean-filtered where indicated. The tunneling parameters are given in the figure captions, with the sign of the voltage referred to the sample.

Results and Discussion

STM imaging revealed large highly ordered domains. Figure 1a depicts a 25×25 nm^2 section of an ordered domain several hundred nanometers in size. In the case of "as grown" layers, isolated excess molecules could frequently be found adsorbed on top of the monolayer. Since these molecules are either moved or picked up by the tip, they lead to tip changes and an unstable imaging process. However, careful annealing after the initial deposition up to approximately 150 °C for 20 min increased the mobility of these excess molecules sufficiently to remove them from the adlayer. This improved the stability of the tip and the imaging process.

Fourier transformations of several drift-corrected (during the measurement) images provide an average length of (1.7 ± 0.1) nm for both adsorbate lattice base vectors and an angle between them of $98 \pm 3°$. Monolayers of Pc's typically exhibit lattice constants that are approximately 0.3 nm smaller than this, almost independent of the substrate.[24−26] Given the "flat" adsorption geometry of most Pc's (i.e., molecular planes parallel to the surface), this suggests the same flat orientation for Nc monolayers. Occasionally, point defects could be observed in the Nc monolayers on HOPG, an example of which is depicted in Figure 1. These vacancies, with their four-leaf-clover shape, resemble the molecular structure and are valuable for a detailed understanding of the image contrast. These missing molecules allow the azimuthal orientation of single Nc's within the layer to be determined. Although in closed layers the position of a single molecule in the STM image can be inferred intuitively, its rotational orientation remains ambiguous. Utilizing the deduced orientation, the STM image can be overlaid with molecular models as shown for one unit cell in Figure 1b. In addition, the angle δ between the molecular axis and the lattice vector can be measured as indicated in Figure 1b. δ was determined to be $29 \pm 3°$ and is only slightly larger than the values observed for different Pc's (between 22 and 28°). Thus, Nc monolayers are found to exhibit a very similar structure to their Pc counterparts.

A very interesting feature of the Nc monolayers is the dependence of the submolecular STM contrast on the bias polarity. For negative sample bias, i.e., tunneling out of occupied sample states, the center of the Nc appears dark, as shown in Figure 1. For positive sample bias, i.e., tunneling into unoccupied sample states, all molecules appear as bright humps,

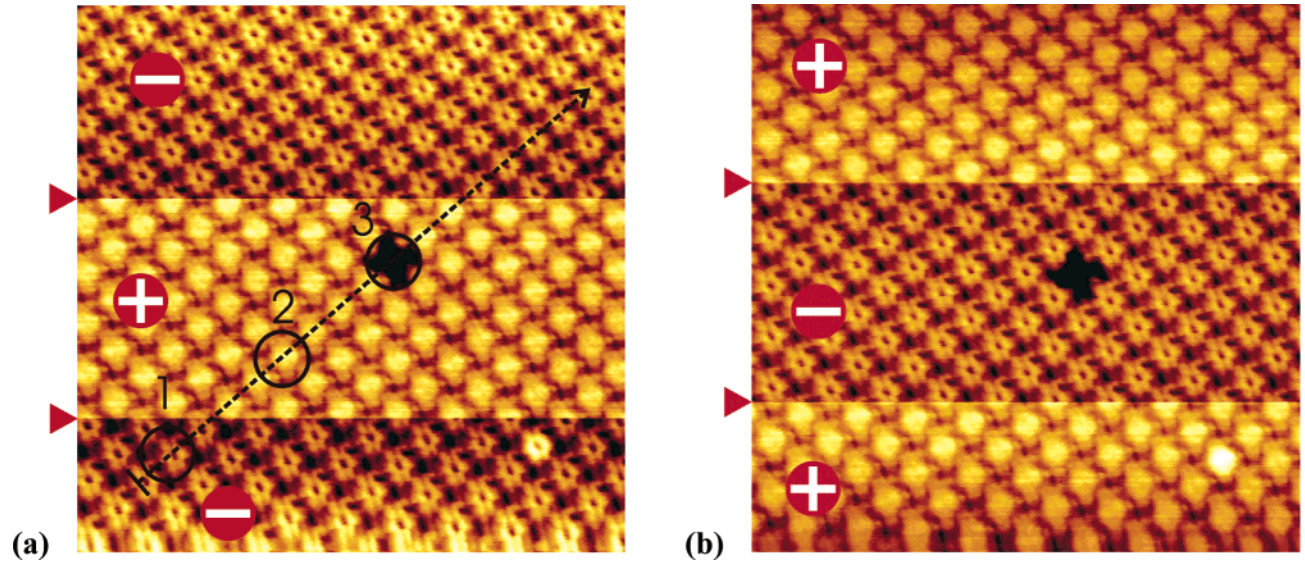

Figure 2. High-resolution STM constant current topographs of a Nc monolayer on HOPG (25×25 nm^2, $|V| = 1.83$ V, 83 pA) obtained at 50 K; during the scans the polarity of the tunneling voltage was switched twice. In a scanning was started with negative sample bias, whereas in b it started with positive sample bias. The corresponding lines where switching took place are marked by triangles on the left-hand side, and the actual sign of the sample bias is given within each part of the frame. Both images represent approximately the same sample area but have a different order of switching. The line, circles, and numbering in a refer to the line scan depicted in Figure 3.

without any indication of a decrease in apparent height at the center. To exclude artifacts due to tip changes, the bias was switched back and forth within a single scanning frame. The topograph in Figure 2a—scanned from bottom to top—was started with negative tunneling voltage. After about one-third of the image was scanned, the polarity was switched, and finally, after two-thirds of the image was scanned, the polarity was switched back to negative sample bias again. Clearly, the two-thirds of the image acquired under the same polarity exhibits the same intramolecular contrast. The appearance of the internal structure was independent of the initial condition and the order of switching, as demonstrated in Figure 2b where the opposite order was employed. For negative sample bias depressions are always observed in the centers of the molecules, whereas for positive sample bias molecules appear with bright bumps in the center. A qualitatively similar change of the intramolecular contrast was found for polarity switching at different biases; however, lower voltages lead to slightly degraded image resolution. Additionally, the change of the internal structure upon polarity switching is accompanied by a sudden change in the mean apparent height of the molecules. In both Figure 2a and b for positive sample bias, all molecules appear higher, i.e., brighter, than for negative sample bias. Yet, the gradual change of the background height right after switching—e.g. visible at the top part of Figure 2a—is an artifact. Possible explanations for this background change are offered by nonideal piezo behavior such as creep or hysteresis. Since these topographs represent raw data, any influence arising from image processing can be discounted.

For a more quantitative representation of the data, a line profile along the black line in Figure 2a has been extracted and is depicted in Figure 3. This line profile has been taken along a lattice vector of the adsorbate layer through the centers of the molecules and includes the switching of the polarity from negative to positive and back to negative sample bias. For positive sample bias the upper edges of the molecules are raised roughly 0.3 Å compared to negative sample bias, whereas the trough between neighboring molecules is hardly affected by the switching. For negative sample bias—a single molecule is marked in Figure 3 by the number 1—the depression in the

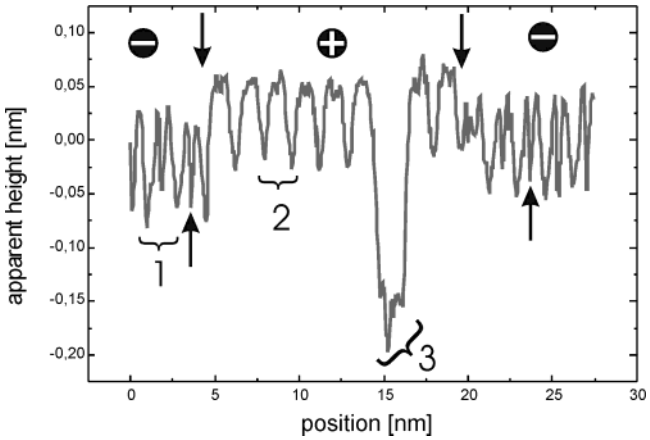

Figure 3. Profile along the line marked in Figure 2a. The upper arrows indicate roughly the positions of the polarity switching; the actual sign of the tunneling voltage is given above the line trace. The numbering refers to Figure 2a and marks single molecules for (1) negative and (2) positive sample bias and (3) the vacancy. Lower arrows at negative bias mark centers of molecules appearing as a depression.

center of the molecule is clearly visible and reaches almost the same depth as the depression between molecules. The vacancy—marked by the number 3—shows a depth of about 2.0 Å for positive sample bias, which is in agreement with the apparent height as observed by STM for monolayers of planar π-conjugated molecules.[27] For negative sample bias the depth of the vacancy amounts to 1.7 Å. The difference in these vacancy depths between positive and negative sample bias reflects the apparent height difference of the occupied and unoccupied states.

As anticipated, the nearest neighbor distance for Nc is enlarged compared to that for Pc's. The lattice parameters are consistent with molecules lying flat, i.e., with the molecular plane parallel to the substrate. This seems reasonable since Nc exhibits a fairly large conjugated electron system and the flat adsorption geometry maximizes the favorable interaction of the π-electronic states with the graphite substrate. Flat adsorption geometries are common for phthalocyanines on a variety of substrates and for many other planar organic molecules with conjugated π-electron systems. The actual size of the unit cell

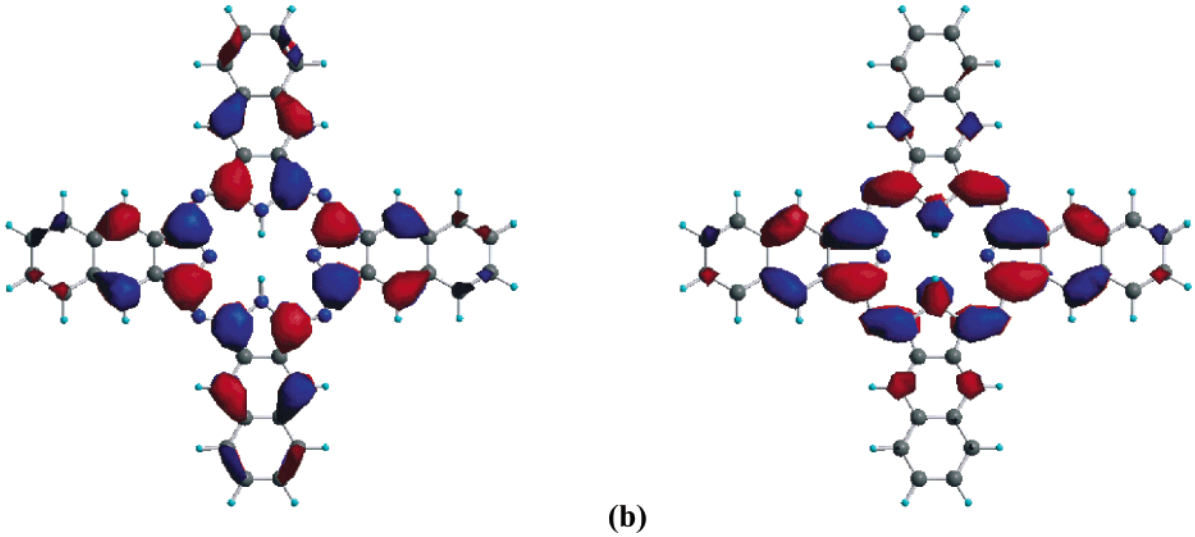

Figure 4. "Restricted-Hartree−Fock" calculation of **(a)** HOMO and **(b)** LUMO for isolated Nc molecules using the GAUSSIAN 98 program package.

is determined by a balance between the (mainly van der Waals) molecule−molecule interactions and molecule−substrate interactions. The increased molecular size of Nc leads primarily to a scaling up of the unit cell observed for a typical Pc monolayer unit cell.

Although for many organic adsorbates on graphite, stable imaging is only possible for one tunneling voltage polarity, in the present case high-resolution images could be obtained for both polarities. A possible explanation for this phenomenon can be found in the electronic structure of Nc with its relatively small HOMO−LUMO gap and a highly delocalized π-electron system in comparison to smaller organic molecules typically investigated by STM. The energy spread of occupied versus unoccupied states, their placement with respect to the graphite Fermi level, and the delocalized spatial distribution are certainly all factors that contribute to this effect. To understand the differences observed upon polarity switching, an interpretation in terms of molecular orbitals is appropriate. In general, STM images acquired with positive sample bias (i.e., with electrons tunneling into the sample) are assumed to access unoccupied sample states, while negative sample bias (i.e., with electrons tunneling out of the sample) involve occupied sample states. Strictly speaking, for image simulations the electronic structure of the coupled adsorbate−substrate system needs to be evaluated and mixing with substrate states should be considered. Since coupling to the graphite substrate is expected to be weak and the interaction among the molecules is restricted to van der Waals forces as well, consideration of isolated, geometry-optimized molecules represents a good first approximation for determining the tunneling behavior. This approach is justified by the assumption that physisorption has little influence on the geometric and electronic structure of the molecule. Even when a contrast modulation due to substrate interactions is observed,[5,28,29] for weakly interacting substrates good agreement between submolecular STM contrast and the frontier molecular orbitals of gas-phase molecules is generally observed.[30] In the present study the wave functions and energies of the molecular orbitals were calculated using the "restricted Hartree−Fock" method with the GAUSSIAN 98 program package. Figure 4 shows the calculated HOMO and LUMO of isolated Nc. The LUMO has electron density at the center of the molecule and at the inner hydrogen atoms, which correlates well with the observed hump (high tunneling probability) in the STM image for positive tunneling voltage. The LUMO+1 is separated from the LUMO by only 300 meV in energy and has a similar spatial structure when rotated by 90°. Since the bonding of the inner hydrogen atoms was fixed for the calculation, no mesomeric effects associated with hydrogen tunneling were considered. Since the two inner hydrogen atoms can alternately bind to the other two pyrrolic nitrogens (see Figure 1a) to create an equivalent configuration (rotated by 90°), a degeneracy of the LUMO and LUMO+1 becomes likely. The vanishing or at least small energy difference between LUMO and LUMO+1 suggests the likelihood that both molecular orbitals (or a linear combination thereof) contribute to the STM image for positive sample bias, thereby explaining the high tunneling current at the center of the molecule. On the other hand the HOMO shows no electron density in the middle of the molecule. Here the center is surrounded by eight electron density maxima situated on a ring. The shape of this wave function is in very good agreement with the central depression observed experimentally at negative sample bias. The HOMO-1 is separated from the HOMO by a rather large energy difference of several electronvolts and, therefore, is believed not to contribute to the observed image contrast. Nevertheless, its shape is also consistent with the experimental results, showing a depression in the middle of the molecule for negative sample bias.

At higher tunneling current the contrast of the Nc molecules is modulated by a striped pattern, depicted in Figure 5a,b. Since the striped pattern is pronounced for smaller tip−sample separations and its periodicity is in the range of the graphite interatomic lattice spacing, this feature is assigned to the substrate. When the tip approaches the surface, contributions of the graphite electronic states to the tunneling current are more likely, and the substrate becomes visible through the organic monolayer. This effect has been observed for many adsorbate−substrate combinations and can be utilized to determine lattice parameters with high accuracy by means of the intrinsic ruler of the underlying substrate.[31−34] Because an increased interaction with the substrate causes the striped pattern, this feature should be highly sensitive to the adsorption site of the molecules. However, all Nc molecules look similar in the images even at larger scan widths; no long-range variation of the apparent height by a Moiré effect is evident. In addition, the relative position of the stripes with respect to the molecule is the same for all Nc's. This is an indication of similar adsorption sites for all the molecules and, therefore, a commensurate superstructure. From the lattice parameters measured in the STM images, a

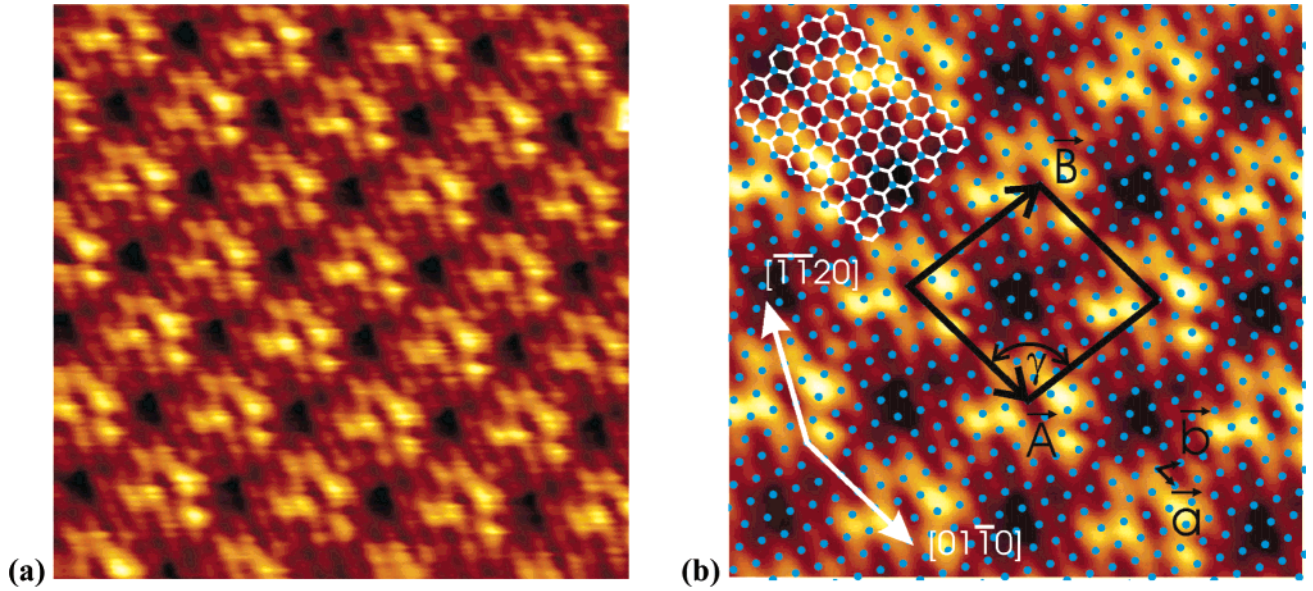

Figure 5. STM image of a Nc monolayer for a small tip−sample separation, i.e., a higher tunneling current (−1.97 V, 0.71 nA, 50 K) than used in Figures 1−3; the image is superimposed with a stripe pattern, which is caused by contributions of the substrate: **(**a**)** mean filtered image (10 × 10 nm^2); **(**b**)** averaged image (6 × 6 nm^2) with overlaid substrate lattice and unit cells. Large and small black arrows represent unit cells of the Nc monolayer ($\vec{A}$, $\vec{B}$) and graphite substrate ($\vec{a}$, $\vec{b}$), respectively; dots represent the hexagonal lattice of the visible graphite B-atoms; the white hexagons placed on the upper left side indicate the topmost layer of graphite. One of the white arrows points along a [-1-120] direction of the substrate, which coincides with the orientation of the stripe pattern; the other one indicates the [01-10] direction, which is parallel to a primitive vector of the B-atom lattice.

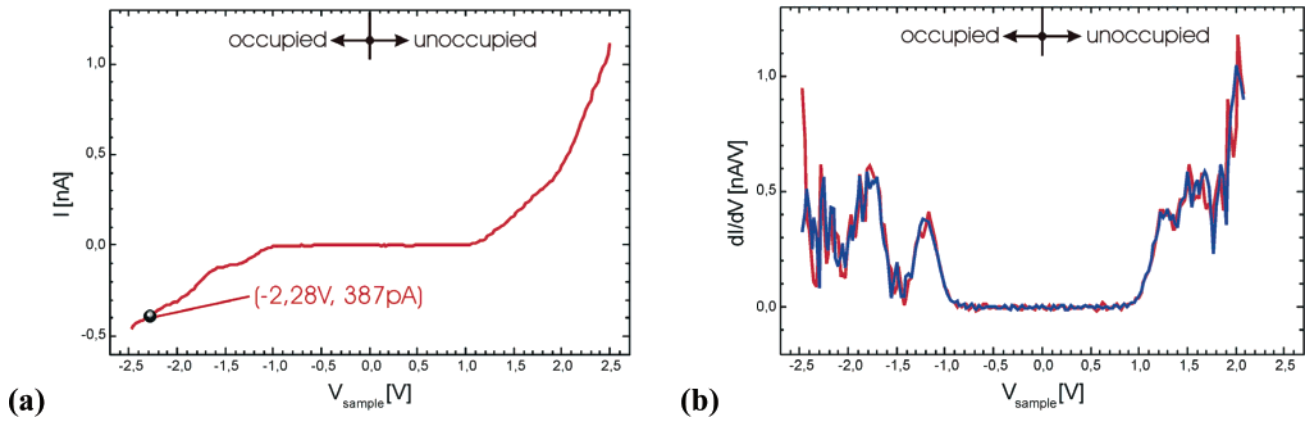

Figure 6. STS of Nc on graphite: **(**a**)** averaged $I-V$ curve obtained by recording 50 single measurement curves; **(**b**)** numerically calculated derivative of the curve in a. To exclude averaging artifacts, the data set has been split into two independent data sets (blue and red curves respectively) of approximately 25 measurements each, which agree quite well with each other. Since the two curves coincide so well, they are difficult to distinguish.

commensurate structure can be constructed by considering different rotations of the unit cell on the graphite mesh. The best match is expressed by the following matrix:

$$\begin{pmatrix}\vec{A}\\ \vec{B}\end{pmatrix} = \begin{pmatrix}7 & 0\\ -3 & 8\end{pmatrix}\begin{pmatrix}\vec{a}\\ \vec{b}\end{pmatrix}$$

using the visible "B-atoms" of the topmost graphite layer as a base. The proposed unit cell with the graphite lattice superimposed is shown in the averaged image of Figure 5b. Several equivalent close ups of a larger periodic topograph were used for the averaging process. The alignment and selection of the single frames was accomplished by means of the cross-correlation of the close-up image with the main image. Further experimental evidence for the proposed commensurate unit cell is that the stripes are oriented parallel to a high-symmetry [-1-120] direction of graphite as indicated by the nearly vertical white arrow in Figure 5b, thereby relating the contrast modulation to the substrate structure. However, the orientation of the Nc unit cell with respect to the graphite substrate and the commensurability cannot be fully proven by STM data alone. LEED measurements of Nc monolayers adsorbed on a natural graphite crystal confirm the alignment of one of the adsorbate vectors with a lattice vector of the graphite B-atom lattice (parallel to the [01-10] direction of graphite).[35]

Further investigation of the local electronic structure has been performed using scanning tunneling spectroscopy (STS). As usual the STM feedback was deactivated for the voltage ramp and the current was recorded. During spectroscopy runs the monolayer was simultaneously imaged with submolecular resolution, thereby allowing $I-V$ curves to be measured at randomly selected points. Figure 6a shows an average of approximately 50 individual $I-V$ curves taken above the center of the molecules. The set point used to stabilize the tunneling gap is also shown in Figure 6a. Additionally, the derivative of this $I-V$ curve has been calculated numerically and is depicted in Figure 6b. First of all, the spectroscopic data indicate

semiconducting behavior with a gap in both the $I-V$ and dI/dV characteristics, as would be expected for an adsorbate with a gap in its electronic structure. Since there is no current measured in the gap region from $-(0.9 \pm 0.1)$ to $+(0.9 \pm 0.1)$ V, a contribution of the substrate states can be excluded for this particular tip−sample distance. The $I-V$ curves are asymmetric with a higher tunneling current measured for positive compared to negative sample bias at the same absolute voltage. This is consistent with the observed height change in constant current mode found upon switching the voltage polarity. As demonstrated in Figures 2a,b, the apparent height of the unoccupied states is larger than that of the occupied states. In the $I-V$ curves the current is larger for positive sample bias, and therefore in constant current mode the tip has to be retracted when switching from negative to positive sample bias. Of course, the height difference between occupied and unoccupied sample states is also dependent on the tunneling voltage. The numerically computed derivative curves shown in Figure 6b exhibit clear maxima of the kind expected for resonant tunneling into molecular orbitals.[36] To test the reproducibility of the dI/dV curve, the data set of 50 $I-V$ curves was split into two independent data sets of equal size. The two curves obtained from these sets show very good agreement, even in the apparent fine structure.

Conclusion

Submolecularly resolved STM images were recorded for free-base Nc monolayers on graphite, allowing the unit cell and the orientation of single molecules to be determined. Molecules were observed to lie flat, and the measured lattice constants are about 0.3 nm larger than those found for phthalocyanines. The internal structure of Nc in STM images is dependent on the polarity of the tunneling voltage. Occupied molecular states exhibit a decrease in the tunneling current at the molecular center, whereas unoccupied states show an increase in tunneling at the center. These differences are consistent with the frontier molecular orbitals calculated for gas-phase molecules. For smaller tip−sample separations contributions of substrate states to the tunneling current lead to a modulation of the image by a striped pattern. The direction of the striped pattern is in accordance with the proposed commensurate unit cell. Tunneling spectroscopy reveals a 1.8 eV wide energy gap in the $I-V$ characteristics and peaks in the dI/dV curves. In summary, STM and STS have been utilized as powerful tools for obtaining detailed insight into the adsorption geometry and local electronic structure of an adsorbate monolayer composed of a versatile model compound of potential interest in the development of molecular devices.

Acknowledgment. This work was supported by the Department of Energy under Grant DE-FG02-88ER13937 and in part by the MRSEC Program of the National Science Foundation under Award No. DMR-02-13574 and by the Nanoscale Science and Engineering Initiative of the National Science Foundation under NSF Award No. CHE-01-17752. Equipment support was provided by the National Science Foundation under Grant CHE-00-95649. M.L. thanks the German Academic Exchange Service (DAAD) for support within its Ph.D. students' program.

References and Notes

(1) Gimzewski, J. K.; Stoll, E.; Schlittler, R. R. *Surf. Sci.* **1987**, *181*, 267−277.
(2) Lippel, P. H.; Wilson, R. J.; Miller, M. D.; Wöll, Ch.; Chiang, S. *Phys. Rev. Lett.* **1989**, *62* (2), 171−174.
(3) Möller, R.; Coenen, R.; Esslinger, A.; Koslowski, B. *J. Vac. Sci. Technol., A* **1990**, *8* (1), 659−660.
(4) Mizutani, W.; Shigeno, M.; Sakakibara, Y.; Kajimura, K.; Ono, M.; Tanishima, S.; Ohno, K.; Toshima, N. *J. Vac. Sci. Technol., A* **1990**, *8* (1), 675−678.
(5) Ludwig, C.; Strohmaier, R.; Petersen, J.; Gompf, B.; Eisenmenger, W. *J. Vac. Sci. Technol., B* **1994**, *12* (3), 1963−1966.
(6) Dekker, C.; Tans, S. J.; Oberndorff, B.; Meyer, R.; Venema, L. C. *Synth. Met.* **1997**, *84*, 853−854.
(7) Kanai, M.; Kawai, T.; Motai, K.; Wang, X. D.; Hashizume, T.; Sakura, T. *Surf. Sci.* **1995**, *329*, L619−623.
(8) Grand, J.-Y.; Kunstmann, T.; Hoffmann, D.; Haas, A.; Dietsche, M.; Seifritz, J.; Möller, R. *Surf. Sci.* **1996**, *366*, 403−414.
(9) Maeda, Y.; Matsumoto, T.; Kasaya, M.; Kawai, T. *Jpn. J. Appl. Phys.* **1996**, *35*, L405−L407.
(10) Nakamura, M.; Morita, Y.; Tokumoto, H. *Appl. Surf. Sci.* **1997**, *113/114*, 316−321.
(11) Böhringer, M.; Berndt, R.; Schneider, W.-D. *Phys. Rev. B* **1997**, *55* (3), 1384−1387.
(12) Hersam, M. C.; Guisinger, N. P.; Lyding, J. W. *J. Vac. Sci. Technol., A* **2000**, *18* (4), 1349−1353.
(13) Hiesgen, R.; Räbisch, M.; Böttcher, H.; Meissner, D. *Sol. Energy Mater. Sol. Cells* **2000**, *61*, 73−85.
(14) Stöhr, M.; Wagner, T.; Gabriel, M.; Weyers, B.; Möller, R. *Adv. Funct. Mater.* **2001**, *11* (3), 175−178.
(15) Lu, X.; Hipps, K. W.; Wang, X. D.; Mazur, U. *J. Am. Chem. Soc.* **1996**, *118*, 7197−7202.
(16) Hipps, K. W.; Lu, X.; Wang, X. D.; Mazur, U. *J. Phys. Chem.* **1996**, *100*, 11207−11210.
(17) Lu, X.; Hipps, K. W. *J. Phys. Chem. B* **1997**, *101*, 5391−5396.
(18) Strohmaier, R.; Ludwig, C.; Petersen, J.; Gompf, B.; Eisenmenger, W. *J. Vac. Sci. Technol., B* **1996**, *14* (2), 1079−1082.
(19) Lackinger, M.; Hietschold, M. *Surf. Sci.* **2002**, *520*, L619−L624.
(20) Magonov, S. N.; Cantow, H.-J.; Ham, D. M. W. v.d. *Synth. Met.* **1991**, *41*−*43*, 2639−2642.
(21) Manivannan, A.; Nagahara, L. A.; Yanagi, H.; Kouzeki, T.; Ashida, M.; Maruyama, Y.; Hashimoto, K.; Fujishima, A. *Thin Solid Films* **1993**, *226*, 6−8.
(22) Nagahara, L. A.; Manivannan, A.; Yanagi, H.; Toriida, M.; Ashida, M.; Maruyama, Y.; Hashimoto, K.; Fujishima, A. *J. Vac. Sci. Technol., A* **1993**, *11* (4), 781−785.
(23) Manivannan, A.; Nagahara, L. A.; Hashimoto, K.; Fujishima, A. *Langmuir* **1993**, *9*, 771−775.
(24) Buchholz, J. C.; Somorjai, G. A. *J. Chem. Phys.* **1977**, *66* (2), 573−580.
(25) England, C. D.; Collins, G. E.; Schuerlein, T. J.; Armstrong, N. R. *Langmuir* **1994**, *10*, 2748−2756.
(26) Yim, S.; Jones, T. S. *Surf. Sci.* **2002**, *521*, 151−159.
(27) Barlow, D. E.; Hipps, K. W. *J. Phys. Chem. B* **2000**, *104*, 5993−6000.
(28) Lackinger, M.; Griessl, S.; Heckl, W. M.; Hietschold, M. *Anal. Bioanal. Chem.* **2002**, *374*, 685−687.
(29) Sellam, F.; Schmitz-Hübsch, T.; Toerker, M.; Mannsfeld, S.; Proehl, H.; Fritz, T.; Leo, K.; Simpson, C.; Müllen, K. *Surf. Sci.* **2001**, *478*, 113−121.
(30) Strohmaier, R.; Petersen, J.; Gompf, B.; Eisenmenger, W. *Surf. Sci.* **1998**, *418*, 91−104.
(31) Hoshino, A.; Isoda, S.; Kurata, H.; Kobayashi, T. *J. Appl. Phys.* **1994**, *76* (7), 4113−4120.
(32) Claypool, C. L.; Faglioni, F.; Goddard, W. A., III; Gray, H. B.; Lewis, N. S.; Marcus, R. A. *J. Phys. Chem. B* **1997**, *101*, 5978−5995.
(33) Walzer, K.; Sternberg, M.; Hietschold, M. *Surf. Sci.* **1998**, *415*, 376−384.
(34) Upward, M. D.; Beton, P. H.; Moriarty, P. *Surf. Sci.* **1999**, *441*, 21−25.
(35) Work in progress.
(36) Hipps, K. W.; Barlow, D. E.; Mazur, U. *J. Phys. Chem. B* **2000**, *104*, 2444−2447.